

Fluorophore-Dapagliflozin Dyad for Detecting Diabetic Liver/Kidney Damages via Fluorescent Imaging and Treating Diabetes via Inhibiting SGLT2

Wenlan Yu,^{||} Jing Huang,^{||} Mingang Lin,^{||} Guimei Wei, Fan Yang, Zhaoxin Tang,^{*} Fang Zeng, and Shuizhu Wu^{*}



Cite This: *Anal. Chem.* 2021, 93, 4647–4656



Read Online

ACCESS |



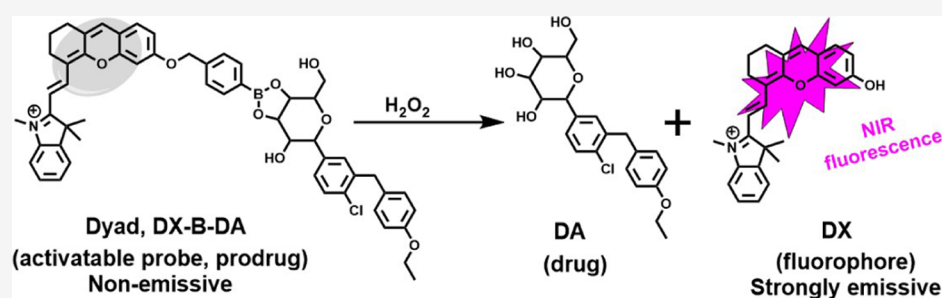
Metrics & More



Article Recommendations



Supporting Information



ABSTRACT: Type II diabetes is a prevalent disease; if left untreated, it could cause serious complications including liver and kidney damages. Hence, early diagnosis for these damages and effective treatment of diabetes are of high importance. Herein, a fluorophore-dapagliflozin dyad (DX-B-DA) has been developed as a theranostic system that can be triggered by intrahepatic/intrarenal reactive oxygen species (ROS) to concomitantly release a near-infrared (NIR) fluorescent dye (DX) and a SGLT2 inhibitor dapagliflozin (DA). In this dyad (DX-B-DA), the NIR fluorophore (DX) and the drug DA were covalently linked through a boronate ester bond which serves as the fluorescence quencher as well as the ROS-responsive moiety that can be cleaved by pathological levels of ROS in diabetics. The *in vitro* experiments indicate that, in the absence of hydrogen peroxide, the dyad is weakly emissive and keeps its drug moiety in an inactive state, while upon responding to hydrogen peroxide, the dyad simultaneously releases the NIR dye and the drug DA, suggesting that it can serve as an activatable probe for detecting and imaging diabetic liver/kidney damages as well as a prodrug for diabetes treatment upon being triggered by ROS. The dyad was then injected in mouse model of type II diabetes, and it is found that the dyad can not only offer visualized diagnosis for diabetes-induced liver/kidney damages but also exhibit high efficacy in treating type II diabetes and consequently ameliorating diabetic liver/kidney damages.

INTRODUCTION

The prevalence of diabetes has been rising globally alongside with the increasing prevalence of obesity; around 10% of adults have diabetes, and about 90% of diabetic patients have type II diabetes.^{1–3} If left undertreated or untreated, diabetes could cause serious complications that could damage vital organs including liver and kidneys and could even lead to premature death.^{2,4–8} Type II diabetes is a great risk factor for serious liver diseases (including nonalcoholic fatty liver disease and even cirrhosis). Type II diabetes and liver diseases are closely associated with severe adverse outcomes, and their bidirectional relationship constitutes a vicious cycle that enhances risks for each other.^{4–6} Diabetic nephropathy is also a common complication for type II diabetes. Diabetes has become the leading cause of kidney diseases, and diabetic kidney disease develops in about 40% of diabetic patients worldwide.^{8,9} As for the development of renal changes in diabetes, the initial period features early hyperfunction, hypertrophy, and increased

urinary albumin excretion, but these changes are reversible by treatment of diabetes.^{8–11} Over time, diabetes can cause damage to blood vessel clusters in kidneys, which will lead to kidney damages such as morphologic lesions and enhanced albumin excretion. If left untreated, renal function further declines, and overt diabetic nephropathy and even end-stage renal failure with uremia might occur. The presence and severity of diabetic liver/kidney diseases are the common causes for enhanced risk of morbidity, adverse outcomes, and premature mortality.^{9–12}

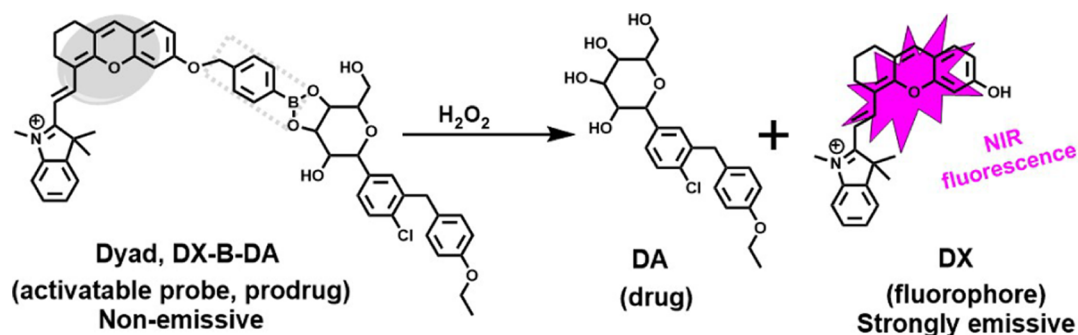
Received: January 17, 2021

Accepted: February 22, 2021

Published: March 4, 2021



Scheme 1. Chemical Structure of Dyad (DX-B-DA) and Its Release of the NIR Fluorophore (DX) and the Drug DA Upon Being Triggered by Hydrogen Peroxide; Gray Dotted Rectangle Indicates the Boronate Ester-Containing Benzyl That is Cleavable in the Presence of H_2O_2



Identifying liver and kidney damages early in the course of diabetes in combination with effective diabetes treatment can ameliorate diabetic liver/kidney damages, help to prevent the onset of serious diabetic liver/kidney diseases, and possibly avoid the progression toward serious liver diseases or end-stage renal failure. This would have quite a positive impact on the diagnosis and treatment of diabetic liver/kidney diseases, decrease the incidence of mortality, and lead to the improved health outcome for diabetic patients. In diabetes, hyperglycemia activates a metabolic route which involves diacylglycerol, protein kinase C and NADPH-oxidase, and culminates in reactive oxygen species (ROS) generation.^{13–15} The generation of ROS has been regarded as the primary initiating event in the development of diabetes complications, and the elevated oxidative stress resulting from the elevated intrahepatic and intrarenal ROS produces direct damage to hepatic cells and podocytes and contribute to the development and progression of liver and kidney damages/diseases.^{5,6,13,14,16,17} Given the pivotal role of ROS in diabetic complications including liver and kidney damages/diseases, the intrahepatic and intrarenal ROS could serve as an effective marker for diabetic liver and kidney damages/diseases. Thus, employing the intrahepatic/intrarenal ROS as both the in situ biomarker and trigger for detecting diabetic liver/kidney diseases and simultaneously releasing the therapeutic drug for diabetes treatment would become an ideal approach for realizing early detection of diabetic liver/kidney damages and efficacious treatment of diabetes, thus ameliorating diabetic liver/kidney damages.

Glycemic control is fundamental to the management of diabetes. As for the treatment of diabetes, type I diabetes is usually managed with insulin and dietary changes/exercise.¹⁸ Type II diabetes may be treated with noninsulin medications. Sodium-glucose cotransporter-2 (SGLT2) proteins are responsible for roughly 90% of filtered glucose reabsorption. In diabetic patients, the SGLT2 is significantly upregulated, enhancing glucose reabsorption and resulting in glucose conservation and prolonged hyperglycemia.^{19,20} Hence, SGLT2 has become an ideal target for the treatment of type II diabetes. As one of the first drugs that took a new approach for glycemic control in adults with type II diabetes, dapagliflozin (DA) is a highly selective inhibitor for SGLT2 that acts by inhibiting this cotransporter and thereby reduces renal reabsorption of glucose and increases urinary glucose excretion and ultimately reduces hyperglycemia.^{21,22} Currently, DA is usually used via oral administration. However, with such systemic administration, in particular, when DA is taken in

relatively high doses, side effects such as genital yeast infections, dehydration, and constipation might occur.^{23,24} If the drug DA could be transformed into a prodrug with which the active drug is only released at the disease site triggered by the in situ biomarker (e.g., in intrarenal region), then on-demand medication could be achieved with the side effects being diminished or avoided.

We envisage that, coupling a near-infrared (NIR) fluorophore with a SGLT2 inhibitor through a ROS-responsive linker could yield a theranostic system. With the action of the intrahepatic/intrarenal ROS, it could not only detect and image diabetic liver/kidney damages but also ensure on-demand drug release and exert effective treatment for type II diabetes, thus rehabilitating diabetic liver/kidney damages. As a proof of concept, we developed a fluorophore-dapagliflozin dyad as the theranostic system (DX-B-DA) that can be triggered by intrahepatic/intrarenal ROS to concomitantly release both the NIR dye (DX) and the drug DA.^{25,26} With apposite structural design, the dyad system can function as an activatable probe for imaging diabetic liver/kidney damages as well as a prodrug that can be triggered by the in situ biomarker for treatment. As shown in Scheme 1, in this dyad (DX-B-DA), the NIR fluorophore (DX) and the drug DA were coupled through a boronate ester bond that serves as the fluorescence quencher as well as the ROS-responsive linker^{27–30} and can be cleaved by pathological levels of intrahepatic/intrarenal ROS in diabetes. Before responding to hydrogen peroxide, the dyad is weakly emissive, while in the presence of intrahepatic/intrarenal hydrogen peroxide, the dyad can simultaneously release the active drug DA for treating type II diabetes via SGLT2 inhibition as well as the NIR fluorophore for imaging the diabetic liver/kidney damages. Compared to visible light, NIR light has less absorption by hemoglobin and water as well as less autofluorescence by tissues; thus, NIR fluorescence imaging can achieve higher performance as opposed to visible-light fluorescence imaging.^{31–47} In this study, the dyad was employed in the mouse model of type II diabetes, and both the NIR imaging and high efficacy against diabetes were realized.

RESULTS AND DISCUSSION

Synthesis of the Dyad and the Dyad's Response toward H_2O_2 . The dyad was synthesized by incorporating a boronic acid-containing benzyloxy onto a NIR fluorophore followed by coupling the anti-diabetes drug DA with the boronic acid moiety through the boronate ester bond, as shown in Scheme S1. The chemical structure of the dyad was

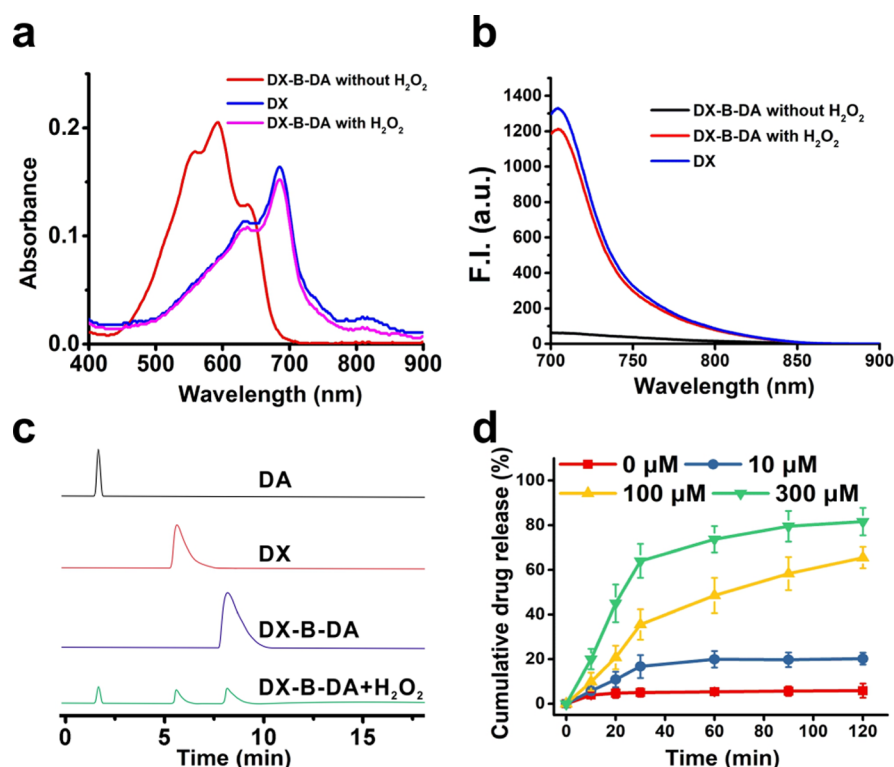


Figure 1. (a) Absorption spectra of the synthesized fluorophore DX, the dyad DX-B-DA in the absence of H₂O₂, and the dyad in the presence of H₂O₂. (b) Fluorescence spectra of the synthesized fluorophore DX, the dyad DX-B-DA in the absence of H₂O₂, and the dyad in the presence of H₂O₂ (500 μM). (c) HPLC chromatograms of the drug DA, the synthesized fluorophore DX, the dyad DX-B-DA, and the dyad in the presence of H₂O₂ (the mobile phase was 75/25 MeCN/H₂O and the flow rate was 1.0 mL/min). (d) Cumulative drug release of the dyad in the presence of different levels of H₂O₂.

characterized by nuclear magnetic resonance and mass spectroscopy, as shown in Figures S1–S6.

The dyad's response toward H₂O₂ was evaluated by absorption and fluorescence spectra. Upon incubation with H₂O₂, the dyad solution's absorption band changes from about 590 nm to around 685 nm (Figure 1a), and the solution changes from the weakly emissive state to the strongly fluorescent state (Figures 1b and S7). As the dyad was incubated with H₂O₂ for different times, its fluorescence intensity increased with the increasing incubation time (Figure S8). It is also evident that the absorption and fluorescence spectra of the dyad after incubation with H₂O₂ are almost the same as those of the fluorophore DX, as shown in Figure 1a,b, suggesting that the product resulting from the reaction between DX-B-DA and H₂O₂ is the fluorophore DX. Upon reaction with H₂O₂, boronate ester-containing benzyl group can be cleaved via self-cleavage reaction.^{26,27,48,49} In order to further confirm the response, high-performance liquid chromatography (HPLC) analysis was conducted. As shown in Figure 1c, the retention time for the drug DA, the fluorophore DX, and the dyad DX-B-DA is 1.7, 5.3, and 8.0 min, respectively. After incubation with H₂O₂, the HPLC peak for the dyad decreases, while the peaks corresponding to DX and DA appear, confirming that the reaction of the dyad with H₂O₂ indeed generates the fluorophore DX and the drug DA. The drug release profiles of the dyad after incubation with different levels of H₂O₂ are displayed in Figure 1d. It can be seen that, in the absence of H₂O₂, almost no drug is released, whereas as the H₂O₂ level is increased, the amount of the released drug increases as well. These data indicate that the

dyad can respond to H₂O₂ and concomitantly release both the fluorescent dye DX and the drug DA.

The limit of detection of the dyad toward H₂O₂ was determined as 0.36 μM (Figure S9). In addition, the dyad's selectivity toward H₂O₂ was investigated experimentally, as shown in Figure S10. It is obvious that the ions, amino acids, and other substances which commonly exist in biological milieu could not interfere with the dyad's response toward H₂O₂. The dyad shows insignificant reactivity to the biologically related oxidizing species such as hypochlorite, superoxide, and hydroxyl radicals, and this result is in consistency with the literature-reported boronate ester-based fluorescent probes for H₂O₂.^{48,49} Hence, the dyad DX-B-DA could serve as a highly selective probe for detecting H₂O₂.

Establishment of Type II Diabetic Mouse Model and Imaging of Diabetic Liver/Kidney Damages by the Dyad DX-B-DA. The C57BL/6J mouse is especially a good model that can mimic human metabolic derangements which are observable in obesity since when fed with high-fat diet (HFD) ad libitum, the mice develop obesity, hypertension, and hyperglycemia, but when fed with chow diet ad libitum, the mice show no metabolic abnormalities and remain lean.^{50,51} Previous research studies have shown that, for C57BL/6J mice, HFD together with a low dose of streptozotocin (STZ) treatment would induce type II diabetes in mice.^{52,53} Hence, in this study, C57BL/6J mice were chosen to establish the mouse model of type II diabetes mellitus. Before being fed with the HFD, oral glucose tolerance test (OGTT) was conducted for the mice which would later be employed to establish the type II diabetes model and compared with the control group. After 12 h of fasting in advance, glucose (2.5 g/kg) was administered

via oral gavage, and then blood glucose levels were tested at different time points, as shown in Figure 2a. It is clear that the

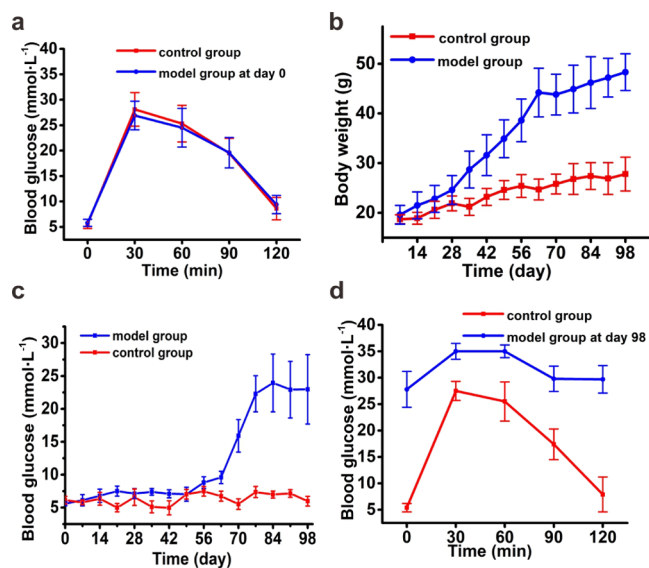


Figure 2. (a) Patterns of blood glucose during OGTT for the control group (healthy mice) and the model group at day 0 (namely, the group intended for HFD). (b) Body weights of the control group and the model group at different time points of the model establishment course. (c) Blood glucose for the control group and the model group at different time points of the model establishment course. (d) Patterns of blood glucose during OGTT for the control group and the model group at day 98 of the model establishment course.

fasting blood glucose levels of the mice peak at about 30 min and return to normal at 2 h, and this demonstrates that before the HFD, the mice are all healthy without diabetes.

In this study, the HFD and low-dose STZ were employed to model type II diabetes. To establish the type II diabetes mouse model, the mice were subject to HFD. At day 63 (9 weeks of HFD), the OGTT results showed glucose tolerance levels for the characterization of mild diabetes (Figure S11), and STZ with a low dose of 50 mg/kg was hence administered via intraperitoneal injection for the mice. When the mean fasting blood glucose was determined to be more than 11.1 mmol/L for 4 weeks, it is considered that type II diabetes has developed in the mice group, and it is referred to as the model group. Compared to the control group (healthy mice with the chow-fed diet) (Figure 2b), upon HFD feeding, the model group's body weight gain continues to be progressively higher, and at day 98, the mice of the model group typically display a 150% increase in body weight. In addition, a significant enhancement in the blood glucose level can be observed for the model group, and hyperglycemia develop upon HFD (98 days) and low-dose STZ administration (at day 63) (Figure 2c). For the model group at day 98 of the model establishment process, OGTT was conducted, and the results were compared with that of the control group. It is obvious that the fasting blood glucose level remains high even 2 h after oral gavage of glucose for the model group, while that of the control group reverts to normal level at 2 h after glucose charge (Figure 2d). Moreover, the typical sign of type II diabetes, including polydipsia, also appears in the model group. The above data confirm that the type II diabetes mouse model has been successfully established.

The serum uric acid that is a predictor of renal injury and the serum creatinine that is widely interpreted as a measure of

the renal function were determined for both the control group (healthy mice group) and the model group (the mice with type II diabetes), as shown in Figure 3a,b. It is clear that, for the model group, the serum uric acid level and the serum creatinine level are higher than those of the control group, indicating that kidney injury occurs in the diabetic mice group. Furthermore, liver function tests were performed via the measurement of blood levels of alanine aminotransferase (ALT) and aspartate aminotransferase (AST), which are two of the enzymes central to identifying liver toxicity, liver disease, or liver damage.^{54,55} As shown in Figure 3c,d, for the model group, the enzymes' levels, especially the ALT level, are much higher than those of the control group, demonstrably indicating that liver damage/injury occurs due to diabetes mellitus. Moreover, lipid blood tests were also conducted for the mice, as shown in Figures S12 and S13. It can be seen that, in the model group, the levels of total blood cholesterol and triglyceride are all higher than those of the control group. The results are consistent with the body weight gain measurement of the model group (Figure 2b) and confirm that the HFD induces obesity and, subsequently, the elevated levels of blood lipids in the mice.

Early in diabetes, hyperglycemia predisposes diabetic patients to glomerular hyperfiltration that results in renal vasodilation, glomerular cells' dysfunction, and cell loss. All of these will lead to diabetic renal injuries and then liver damages and even severe liver/kidney diseases eventually.^{4–6,13–15,56,57} After the type II diabetes mouse model was established, the dyad as the activatable probe was used to image the diabetic liver and kidney damages in the mouse model. Before the imaging, the biosafety of the dyad was evaluated by monitoring the body weights and by performing the histological analysis (H&E staining) of the tissue sections of the major organs of the healthy mice groups with or without i.v. injection of the dyad. As shown in Figure S14, the body weights of the mice groups with or without i.v. injection of the dyad are quite similar, suggesting the low toxicity of the dyad. Moreover, as displayed in Figure S15, as for the H&E staining histological analysis of the tissue sections from the main organs of the healthy mice, there is no obvious difference between the mice group without administration of the dyad and the group i.v. injected with the dyad. These results indicate that the dyad has good biosafety.

Prior to fluorescent imaging, the mice were depilated with depilation cream. Upon i.v. injection of the dyad solution, the mice underwent fluorescent imaging (excitation filter: 670 nm, emission filter: 710 nm). In the imaging experiments, the mice were put in a prone pose under the imaging system, so as to allow better visualization of the kidneys; on the other hand, the mice were also put in a supine position during imaging for a better view of the liver, intestines, and bladder regions. As shown in Figure 3e, when being imaged in a prone position, for the control group, upon i.v. injection of the dyad solution, almost no fluorescence signal appears in the kidney region. In contrast, for the model group (imaged in a prone position), before injection of the dyad solution, almost no fluorescence signal could be observable in the kidney regions, and the fluorescence signals appear in the two kidneys and gradually increase to the maximum at around 10 min upon i.v. injection of the dyad solution (Figure 3e). The appearance of the fluorescent signal indicates that the renal ROS (H_2O_2) that results from the diabetic kidney damages activates the dyad probe and releases the active dye DX molecules which emit

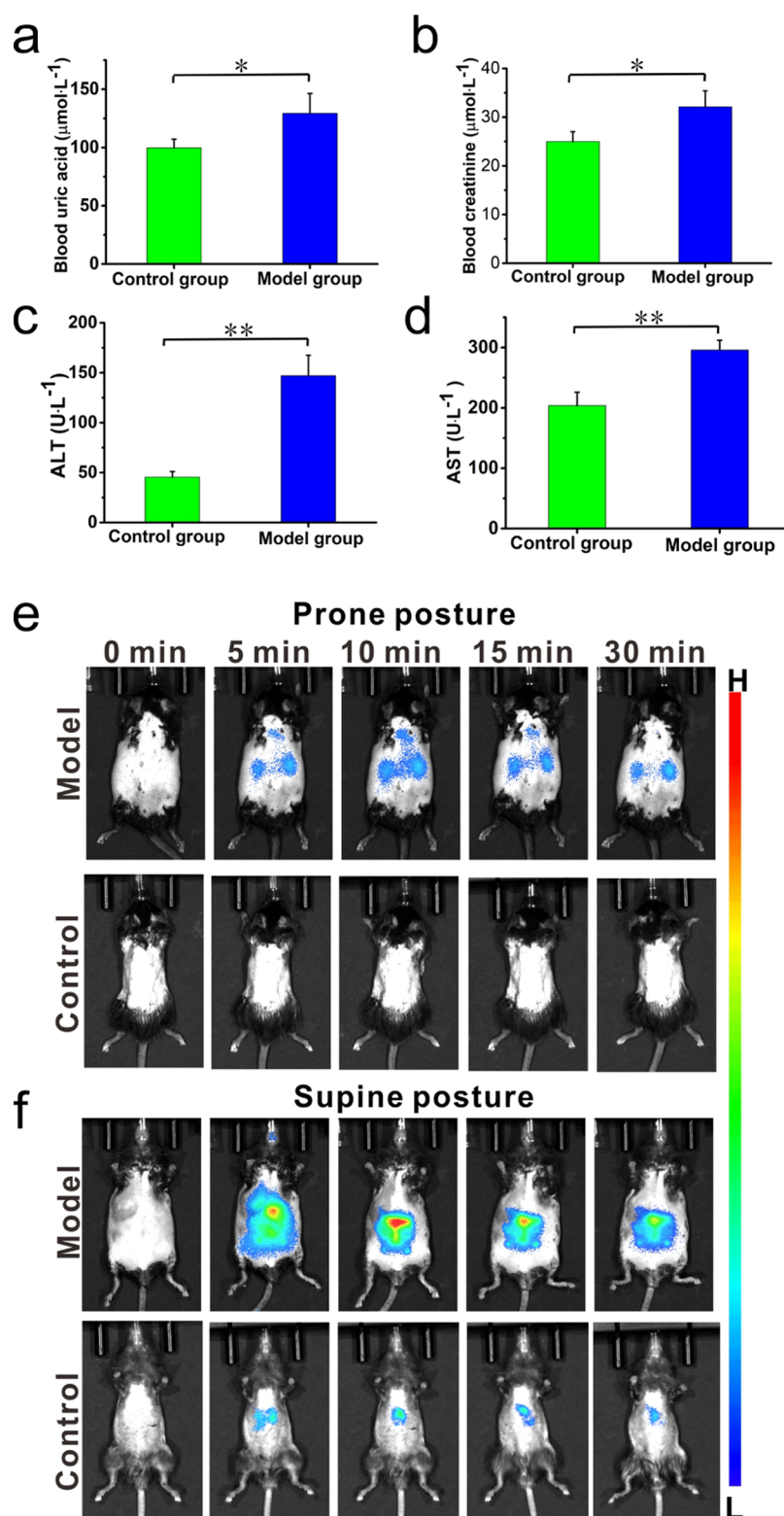


Figure 3. (a) Blood uric acid levels of the control group (healthy mice) and the model group at day 98 of the model establishment course; (b) blood creatinine levels of the control group and the model group at day 98 of the model establishment course; (c) blood ALT levels of the control group and the model group at day 98 of the model establishment course; (d) blood AST levels of the control group and the model group at day 98; (e) fluorescent images in prone posture of the control group and the model group (at day 98) upon i.v. injection of the dyad; (f) fluorescent images in supine posture of the control group and the model group (at day 98) upon i.v. injection of the dyad. Excitation filter (band pass): 670 nm, emission filter (high pass): 710 nm. ** $p < 0.01$, * $p < 0.05$.

fluorescence. The decrease of the fluorescent signal later on is probably due to the metabolism process. When the mice were put in a supine position, as shown in Figure 3f, for the control

group (healthy mice), weak fluorescent signals could be observed in the liver region because there exists a small amount of ROS including H_2O_2 in the healthy liver.^{58–60} In

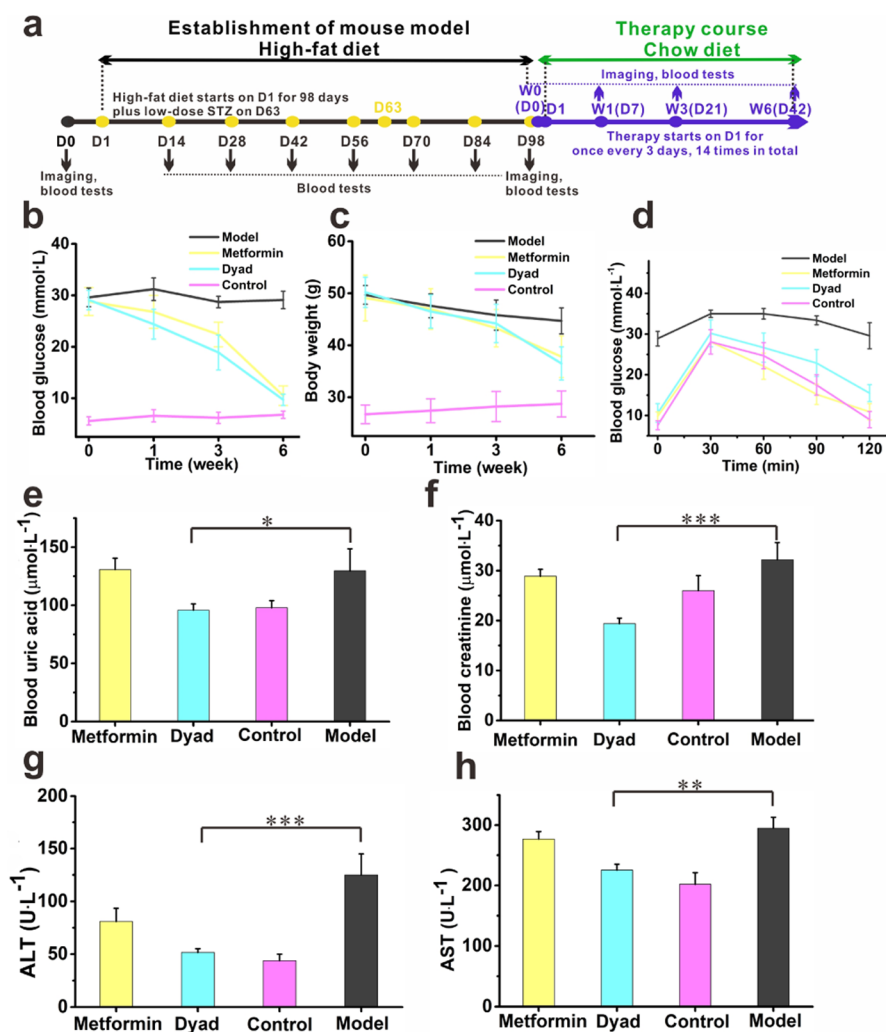


Figure 4. (a) Time course for establishment of the type II diabetic mouse model and therapy course; (b) blood glucose levels of the healthy mice group (designated as control), the model group without treatment (designated as model), the model group upon being treated with metformin (designated as metformin), and the model group upon being treated with the dyad (designated as dyad); (c) body weights of different groups; (d) glucose tolerance test data of different groups at week 6 of the therapy course; (e) blood creatinine levels of different groups at week 6 of the therapy course; (f) blood uric acid levels of different groups at week 6 of the therapy course; (g) blood ALT levels of different groups at week 6 of the therapy course; (h) blood AST levels of different groups at week 6 of the therapy course. Excitation filter (band pass): 670 nm, emission filter (high pass): 710 nm. *** $p < 0.001$, ** $p < 0.01$, * $p < 0.05$.

contrast, evident fluorescent signals were observable in the liver region for the mice of the diabetes model (the model group) in the supine position (Figure 3f). The quantified data for the imaging results (Figure 3e,f) are displayed in Figure S16. These indicate that the dyad molecules are activated by the overexpressed H_2O_2 in the liver and thus give out fluorescent emission. This is because diabetic mellitus also induces damages to the liver besides the kidneys, and consequently, ROS is upregulated.^{4,5}

Therapy of Type II Diabetes and Tracking Rehabilitation of Diabetic Kidney/Liver Damages in the Mouse Model by the Dyad DX-B-DA via Fluorescent Imaging.

To evaluate the capability of the dyad to treat type II diabetes, the mouse model with type II diabetes was established as mentioned above, and the model establishment course and the therapy course are illustrated in Figure 4a. DX-B-DA solution ($4.0 \text{ mg}\cdot\text{kg}^{-1}$) was administered via i.v. injection into the mice group with type II diabetes once every 3 days for 6 weeks (14 times in total, as shown in Figure 4a). For comparison, metformin, a commonly used drug for treatment of type II

diabetes, was administered as well at the dosage of $200 \text{ mg}/\text{kg}$ via intragastric administration once every day for 6 weeks. During the therapy course, the mice were reverted to normal diet. One group of healthy mice was used as the control (designated as control), one model group (diabetic mice) without treatment was employed for comparison (designated as model), one model group received metformin treatment (designated as metformin), and one model group received the dyad treatment (designated as dyad). As for the mice subjected to therapy with the dyad, the blood glucose levels gradually decrease to the level similar to that of the control (healthy mice) (Figure 4b), while the blood glucose of the mice without treatment remained high. After 6 weeks of therapy, the mice's body weight also decreases (Figure 4c). OGTT also shows that, after treatment, the mice display a pattern similar to that of the healthy mice (Figure 4d). As for the mice without therapy (model), the mice still show typical symptoms of diabetes, including high blood glucose and impaired glucose tolerance.

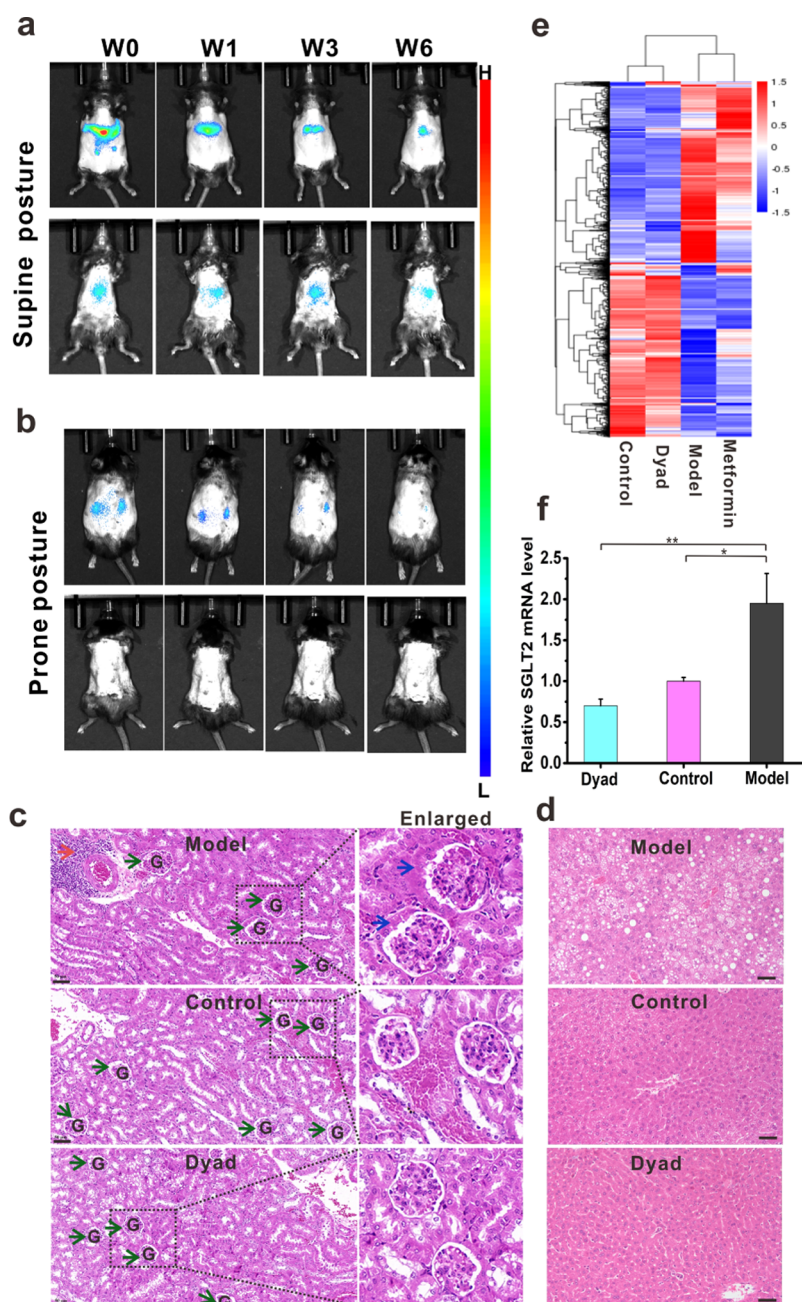


Figure 5. (a) Fluorescent images in supine posture of the control group and the model group at week 0 (before therapy) and weeks 1, 3, and 6 (therapy course) 15 min after i.v. injection of the dyad. (b) Fluorescent images in prone posture of the control group and the model group at week 0 (before therapy) and weeks 1, 3, and 6 (therapy course) 15 min after i.v. injection of the dyad. (c) Histological analysis of tissue sections from the kidneys of the model group (without treatment), the control group (healthy mice), and the dyad group (the diabetic mice group receiving dyad treatment at week 6 of the therapy course). G: glomerulus; green arrow: bowmen's capsule; red arrow: inflammatory cells; blue arrow: cellular crescents. Scale bar: 50 μm . (d) Histological analysis of tissue sections from the livers of the model group (without treatment), the control group (healthy mice), and the dyad group (the diabetic mice group receiving dyad treatment at week 6 of the therapy course). (e) Heatmap and hierarchical cluster analysis showing up-regulated or down-regulated genes for the model group (without treatment), the control group (healthy mice), the dyad group (the diabetic mice group receiving dyad treatment at week 6 of the therapy course), and the metformin group (the diabetic mice group receiving metformin treatment at week 6 of the therapy course). The data tables are graphically presented as colored images (red color indicates up-regulation of gene expression, and blue color indicates down-regulation of gene expression). (f) Relative SGLT2 mRNA levels (measured by RT-qPCR) of the model group (without treatment), the control group (healthy mice), and the dyad group (the diabetic mice group receiving dyad treatment at week 6 of the therapy course). * $p < 0.05$; ** $p < 0.01$.

In order to confirm the rehabilitation of the liver and kidney injuries in the mice after therapy, blood tests for liver and kidney functions and lipid blood tests were conducted, as shown in Figure 4e–h. It can be seen that, compared to the diabetic mice group without treatment (model), after 6 weeks

of therapy, for the group receiving dyad treatment, the levels of blood uric acid, creatinine, ALT, and AST all decrease to the levels congruent with the healthy mice (control) (Figure 4e–h), demonstrating that the kidney and liver functions of the mice upon dyad treatment are largely ameliorated. The blood

lipid test results display a similar pattern and are consistent with the body weight changes of the dyad treatment group (Figure S17). From these results, it is clear that the dyad's therapeutical efficacy for diabetes is comparable to metformin (Figure 4b–d), while the dyad's therapeutic efficacy for the diabetic liver/kidney damages is better than metformin (Figure 4e–h).

After the therapy, fluorescent imaging was performed at 15 min after the mice were i.v. injected with the dyad solution. For the imaging in supine posture, the fluorescent signals in the liver region of the diabetic mice group decrease (Figure 5a) after 6 weeks of dyad treatment and are commensurate with the healthy mice. This indicates that almost no liver injury exists after therapy. As for the imaging in prone posture, it is obvious that the fluorescent signals in the kidneys of the diabetic mice group decrease significantly with almost no observable fluorescent signal, and this suggests that the kidney injury has been greatly ameliorated after therapy (Figure 5b). The quantified data for the imaging results for the prone posture are displayed in Figure S18.

To further confirm the rehabilitation effect on the diabetic kidney and liver damages by the dyad, the tissue sections of the kidney and liver from the diabetic mice (the model group), the healthy mice (the control group), and the mice receiving dyad treatment (the dyad group) were subject to histological analysis (H&E staining), as shown in Figure 5d,e. From Figure 5d, it can be seen that, for the model group (diabetic without receiving treatment), the increase of the glomeruli size is pathophysiologically significant with cellular crescents, and there exists inflammatory cell infiltration, whereas for the dyad group (diabetic mice receiving dyad treatment), the morphology of the glomeruli reverts to normal and is similar to that of the control group (healthy mice). In Figure 5e, it is clear that, for the model group (diabetic mice without receiving treatment), there exist lipid droplets in the liver tissue, while for the dyad group (diabetic mice group receiving dyad treatment), normal hepatocellular morphology can be observed, which is similar to that of the control group (healthy mice). In addition, the SGLT2 levels in the renal tissue lysate were also measured by the Elisa kit, as shown in Figure S19. It is clear that the SGLT2 level is relatively high in the model group (diabetic mice without treatment), while for the dyad group (diabetic mice receiving dyad treatment), the SGLT2 level of the mice decreases to the level comparable to that of the control group (healthy mice). Taken together, it is demonstrably clear that the dyad can serve as an efficacious treatment drug for type II diabetes and thus can greatly ameliorate diabetic liver and kidney damages.

Since RNA expression profiling in renal tissues could function as a prognostic tool for kidney damage/disease,^{61–63} in this study, for the kidney tissues, total RNA extraction and analysis were conducted, so as to confirm the rehabilitating effect of the dyad for diabetic kidney damages from a different perspective. The volcano plots of the gene expression for different mice groups are shown in Figure S20. The Kyoto Encyclopedia of Genes and Genomes pathway analysis of mRNAs is shown in Figure S21. The results not only indicate that the carbon/fatty acid metabolism and the oxidative phosphorylation pathways are coregulated during the occurrence and treatment of diabetes but also demonstrate that oxidative damage is aggravated and energy metabolism is disturbed in diabetic mice, while oxidative damage is reduced and energy metabolism is recovered after dyad treatment.

Hierarchical cluster analyses of the differentially expressed genes were performed as well. As shown in Figure 5e, for the dyad treatment group, the up-regulation and down-regulation profiling of genes are similar to those of the control group (healthy mice), indicating that after the dyad therapy, the wellbeing of the mice with type II diabetes is similar to that of the control group (healthy mice). Moreover, real-time fluorescence quantitative polymerase chain reaction (RT-qPCR) was conducted to evaluate the relative SGLT2 mRNA expression levels in kidney tissues, and the results are shown in Figure 5f. It is clear that, for the model group (diabetic mice), the relative SGLT2 mRNA expression level is almost twice as that of the control (healthy mice), while after the dyad treatment, the relative SGLT2 mRNA expression level decreases significantly. The results further confirm the dyad's therapeutic efficacy for diabetic kidney damage.

CONCLUSIONS

DX-B-DA has been designed as the theranostic system for type II diabetes. The salient feature of this dyad lies in that, upon being triggered by the in situ biomarker (overexpressed intrahepatic/intrarenal ROS), it can simultaneously release the NIR dye (DX) for imaging diabetic kidney/liver damages and the active drug (DA) for treating type II diabetes via inhibiting SGLT2 and consequently ameliorating diabetes-induced liver/kidney damages, thereby acting as both an activatable probe and a therapeutic system. Therefore, the dyad can offer visualized diagnosis for diabetes-induced kidney/liver damages as well as treatment for type II diabetes and diabetic kidney/liver damages. The strategy herein could offer beneficial insights for devising other visualizable theranostic systems for various diseases.

ASSOCIATED CONTENT

Supporting Information

The Supporting Information is available free of charge at <https://pubs.acs.org/doi/10.1021/acs.analchem.1c00223>.

Supplementary experimental section, fluorescence spectra, blood chemical parameters, H&E staining analysis, and volcano plots of differential gene expression (PDF)

AUTHOR INFORMATION

Corresponding Authors

Zhaoxin Tang – College of Veterinary Medicine, South China Agricultural University, Guangzhou 510642, China; Email: tangzx@scau.edu.cn; Fax: +86 20 22236262

Shuizhu Wu – State Key Laboratory of Luminescent Materials and Devices, Guangdong Provincial Key Laboratory of Luminescence from Molecular Aggregates, College of Materials Science and Engineering, South China University of Technology, Guangzhou 510640, China; orcid.org/0000-0002-6739-0694; Email: shzhwu@scut.edu.cn

Authors

Wenlan Yu – College of Veterinary Medicine, South China Agricultural University, Guangzhou 510642, China

Jing Huang – State Key Laboratory of Luminescent Materials and Devices, Guangdong Provincial Key Laboratory of Luminescence from Molecular Aggregates, College of Materials Science and Engineering, South China University of Technology, Guangzhou 510640, China

Mingang Lin – State Key Laboratory of Luminescent Materials and Devices, Guangdong Provincial Key Laboratory of Luminescence from Molecular Aggregates, College of Materials Science and Engineering, South China University of Technology, Guangzhou 510640, China

Guimei Wei – State Key Laboratory of Luminescent Materials and Devices, Guangdong Provincial Key Laboratory of Luminescence from Molecular Aggregates, College of Materials Science and Engineering, South China University of Technology, Guangzhou 510640, China

Fan Yang – Jiangxi Provincial Key Laboratory for Animal Health, Institute of Animal Population Health, College of Animal Science and Technology, Jiangxi Agricultural University, Nanchang 330045, China

Fang Zeng – State Key Laboratory of Luminescent Materials and Devices, Guangdong Provincial Key Laboratory of Luminescence from Molecular Aggregates, College of Materials Science and Engineering, South China University of Technology, Guangzhou 510640, China; orcid.org/0000-0002-6607-3494

Complete contact information is available at:
<https://pubs.acs.org/10.1021/acs.analchem.1c00223>

Author Contributions

[¶]W.Y., J.H., and M.L. contributed equally to this work.

Notes

The authors declare no competing financial interest.

ACKNOWLEDGMENTS

This work was supported by the National Natural Science Foundation of China (21788102 and 21875069), the Natural Science Foundation of Guangdong Province (2016A030312002), and the Fund of Guangdong Provincial Key Laboratory of Luminescence from Molecular Aggregates (2019B030301003).

REFERENCES

- (1) Zheng, Y.; Ley, S. H.; Hu, F. B. *Nat. Rev. Endocrinol.* **2018**, *14*, 88–98.
- (2) Magliano, D. J.; Islam, R. M.; Barr, E. L. M.; Gregg, E. W.; Pavkov, M. E.; Harding, J. L.; Tabesh, M.; Koye, D. N.; Shaw, J. E. *Br. Med. J.* **2019**, *366*, l5003.
- (3) Shaw, J. E.; Sicree, R. A.; Zimmet, P. Z. *Diabetes Res. Clin. Pract.* **2010**, *87*, 4–14.
- (4) Loria, P.; Lonardo, A.; Anania, F. *Hepatol. Res.* **2013**, *43*, 51–64.
- (5) Tolman, K. G.; Fonseca, V.; Dalpiaz, A.; Tan, M. H. *Diabetes Care* **2007**, *30*, 734–743.
- (6) El-serag, H. B.; Everhart, J. E. *Gastroenterology* **2002**, *122*, 1822–1828.
- (7) Blendea, M. C.; Thompson, M. J.; Malkani, S. *Clin. Diabetes* **2010**, *28*, 139–144.
- (8) Alicic, R. Z.; Rooney, M. T.; Tuttle, K. R. *Clin. J. Am. Soc. Nephrol.* **2017**, *12*, 2032–2045.
- (9) Reidy, K.; Kang, H. M.; Hostetter, T.; Susztak, K. *J. Clin. Invest.* **2014**, *124*, 2333–2340.
- (10) Tonneijck, L.; Muskiet, M. H. A.; Smits, M. M.; Van Bommel, E. J.; Heerspink, H. J. L.; Van Raalte, D. H.; Joles, J. A. *J. Am. Soc. Nephrol.* **2017**, *28*, 1023–1039.
- (11) Kato, M.; Natarajan, R. *Nat. Rev. Nephrol.* **2019**, *15*, 327–345.
- (12) Thomas, M. C.; Brownlee, M.; Susztak, K.; Sharma, K.; Jandeleit-Dahm, K. A.; Zoungas, S.; Rossing, P.; Groop, P. H.; Cooper, M. E. *Nat. Rev. Dis. Primers* **2015**, *1*, 15018.
- (13) Volpe, C. M. O.; Villar-Delfino, P. H.; dos Anjos, P. M. F.; Nogueira-Machado, J. A. *Cell Death Dis.* **2018**, *9*, 119.

(14) Jha, J. C.; Banal, C.; Chow, B. S. M.; Cooper, M. E.; Jandeleit-Dahm, K. *Antioxid. Redox Signaling* **2016**, *25*, 657–684.

(15) Singh, D. K.; Winocour, P.; Farrington, K. *Nat. Rev. Endocrinol.* **2011**, *7*, 176–184.

(16) Yao, D.; Brownlee, M. *Diabetes* **2010**, *59*, 249–255.

(17) Forbes, J. M.; Coughlan, M. T.; Cooper, M. E. *Diabetes* **2008**, *57*, 1446–1454.

(18) Atkinson, M. A.; Eisenbarth, G. S.; Michels, A. W. *Lancet* **2014**, *383*, 69–82.

(19) Heerspink, H. J. L.; Perkins, B. A.; Fitchett, D. H.; Husain, M.; Cherney, D. Z. I. *Circulation* **2016**, *134*, 752–772.

(20) Beitelshes, A. L.; Leslie, B. R.; Taylor, S. I. *Diabetes* **2019**, *68*, 1109–1120.

(21) List, J. F.; Woo, V.; Morales, E.; Tang, W.; Fiedorek, F. T. *Diabetes Care* **2009**, *32*, 650–657.

(22) Shah, N. K.; Deeb, W. E.; Choksi, R.; Epstein, B. J. *Pharmacotherapy* **2012**, *32*, 80–94.

(23) Anderson, S. L. *Ther. Adv. Drug Saf.* **2014**, *5*, 242–254.

(24) Donnan, J. R.; Grandy, C. A.; Chibrikov, E.; Marra, C. A.; Aubrey-Bassler, K.; Johnston, K.; Swab, M.; Hache, J.; Curnew, D.; Nguyen, H.; Gamble, J.-M. *BMJ Open* **2019**, *9*, No. e022577.

(25) Han, S.; Hagan, D. L.; Taylor, J. R.; Xin, L.; Meng, W.; Biller, S. A.; Wetterau, J. R.; Washburn, W. N.; Whaley, J. M. *Diabetes* **2008**, *57*, 1723–1729.

(26) Ghezzi, C.; Yu, A. S.; Hirayama, B. A.; Kepe, V.; Liu, J.; Scafoglio, C.; Powell, D. R.; Huang, S.-C.; Satyamurthy, N.; Barrio, J. R.; Wright, E. M. *J. Am. Soc. Nephrol.* **2017**, *28*, 802–810.

(27) Saravanakumar, G.; Kim, J.; Kim, W. J. *Adv. Sci.* **2017**, *4*, 1600124.

(28) Van de Bittner, G. C.; Dubikovskaya, E. A.; Bertozzi, C. R.; Chang, C. J. *Proc. Natl. Acad. Sci. U.S.A.* **2010**, *107*, 21316–21321.

(29) Wang, J.; Liu, L.; Xu, W.; Yang, Z.; Yan, Y.; Xie, X.; Wang, Y.; Yi, T.; Wang, C.; Hua, J. *Anal. Chem.* **2019**, *91*, 5786–5793.

(30) Yu, C.; Li, X.; Zeng, F.; Zheng, F.; Wu, S. *Chem. Commun.* **2013**, *49*, 403–405.

(31) Ding, Q.; Tian, Y.; Wang, X.; Li, P.; Su, D.; Wu, C.; Zhang, W.; Tang, B. *J. Am. Chem. Soc.* **2020**, *142*, 20735–20743.

(32) Zhou, Y.; Li, P.; Wang, X.; Wu, C.; Fan, N.; Liu, X.; Wu, L.; Zhang, W.; Zhang, W.; Liu, Z.; Tang, B. *Chem. Sci.* **2020**, *11*, 12149–12156.

(33) Tian, Y.; Li, Y.; Wang, W.-X.; Jiang, W.-L.; Fei, J.; Li, C.-Y. *Anal. Chem.* **2020**, *92*, 4244–4250.

(34) Ouyang, J.; Sun, L.; Zeng, Z.; Zeng, C.; Zeng, F.; Wu, S. *Angew. Chem., Int. Ed.* **2020**, *59*, 10111–10121.

(35) Wu, Y.; Huang, S.; Wang, J.; Sun, L.; Zeng, F.; Wu, S. *Nat. Commun.* **2018**, *9*, 3983.

(36) Feng, Y.; Jiang, N.; Zhu, D.; Su, Z.; Bryce, M. R. *J. Mater. Chem. C* **2020**, *8*, 11540–11545.

(37) Tian, Y.; Li, Y.; Jiang, W.-L.; Zhou, D.-Y.; Fei, J.; Li, C.-Y. *Anal. Chem.* **2019**, *91*, 10901–10907.

(38) Tian, X.; Yan, F.; Zheng, J.; Cui, X.; Feng, L.; Li, S.; Jin, L.; James, T. D.; Ma, X. *Anal. Chem.* **2019**, *91*, 15840–15845.

(39) Qi, Y.; Huang, Y.; Li, B.; Zeng, F.; Wu, S. *Anal. Chem.* **2018**, *90*, 1014–1020.

(40) Ou-Yang, J.; Li, Y.; Jiang, W.-L.; He, S.-Y.; Liu, H.-W.; Li, C.-Y. *Anal. Chem.* **2019**, *91*, 1056–1063.

(41) Li, W.; Ma, J.; Jiang, Q.; Zhang, T.; Qi, Q.; Cheng, Y. *Anal. Chem.* **2020**, *92*, 3787–3794.

(42) He, L.; Xiong, H.; Wang, B.; Zhang, Y.; Wang, J.; Zhang, H.; Li, H.; Yang, Z.; Song, X. *Anal. Chem.* **2020**, *92*, 11029–11034.

(43) Cho, M. K.; Seo, M. J.; Juvekar, V.; Jo, J. H.; Kim, W.; Choi, K. S.; Kim, H. M. *Anal. Chem.* **2020**, *92*, 11223–11231.

(44) Long, L.; Han, Y.; Liu, W.; Chen, Q.; Yin, D.; Li, L.; Yuan, F.; Han, Z.; Gong, A.; Wang, K. *Anal. Chem.* **2020**, *92*, 6072–6080.

(45) Wang, N.; Yu, X.; Deng, T.; Zhang, K.; Yang, R.; Li, J. *Anal. Chem.* **2020**, *92*, 583–587.

(46) Han, W.; Du, Y.; Song, M.; Sun, K.; Xu, B.; Yan, F.; Tian, W. J. *Mater. Chem. B* **2020**, *8*, 9544–9554.

- (47) Zeng, Z.; Ouyang, J.; Sun, L.; Zeng, C.; Zeng, F.; Wu, S. *Anal. Chem.* **2020**, *92*, 9257–9264.
- (48) Miller, E. W.; Albers, A. E.; Pralle, A.; Isacoff, E. Y.; Chang, C. J. *J. Am. Chem. Soc.* **2005**, *127*, 16652–16659.
- (49) Lin, V. S.; Dickinson, B. C.; Chang, C. J. *Methods Enzymol.* **2013**, *526*, 19–43.
- (50) Collins, S.; Martin, T. L.; Surwit, R. S.; Robidoux, J. *Physiol. Behav.* **2004**, *81*, 243–248.
- (51) Wang, C.-Y.; Liao, J. K. *Methods Mol. Biol.* **2012**, *821*, 421–433.
- (52) Mansor, L. S.; Gonzalez, E. R.; Cole, M. A.; Tyler, D. J.; Beeson, J. H.; Clarke, K.; Carr, C. A.; Heather, L. C. *Cardiovasc. Diabetol.* **2013**, *12*, 136.
- (53) Srinivasan, K.; Viswanad, B.; Asrat, L.; Kaul, C. L.; Ramarao, P. *Pharmacol. Res.* **2005**, *52*, 313–320.
- (54) Giannini, E. G.; Testa, R.; Savarino, V. *Can. Med. Assoc. J.* **2005**, *172*, 367–379.
- (55) Kim, W. R.; Flamm, S. L.; Di Bisceglie, A. M.; Bodenheimer, H. C., Jr. *Hepatology* **2008**, *47*, 1363–1370.
- (56) Hirschberg, R.; Brunori, G.; Kopple, J. D.; Guler, H.-P. *Kidney Int.* **1993**, *43*, 387–397.
- (57) Hirschberg, R.; Kopple, J. D. *J. Am. Soc. Nephrol.* **1992**, *2*, 1417–1422.
- (58) Zorov, D. B.; Juhaszova, M.; Sollott, S. J. *Physiol. Rev.* **2014**, *94*, 909–950.
- (59) Arauz, J.; Ramos-Tovar, E.; Muriel, P. *Ann. Hepatol.* **2016**, *15*, 160–173.
- (60) Azzimato, V.; Jager, J.; Chen, P.; Morgantini, C.; Levi, L.; Barreby, E.; Sulen, A.; Oses, C.; Willerbrords, J.; Xu, C.; Li, X.; Shen, J. X.; Akbar, N.; Haag, L.; Ellis, E.; Wälhen, K.; Näslund, E.; Thorell, A.; Choudhury, R. P.; Lauschke, V. M.; Rydén, M.; Craige, S. M.; Aouadi, M. *Sci. Transl. Med.* **2020**, *12*, No. eaaw9709.
- (61) Eikmans, M.; Baelde, H. J.; Hagen, C.; Paul, L. C.; Eilers, P. H. C.; De Heer, E.; Bruijn, J. *J. Am. Soc. Nephrol.* **2003**, *14*, 899–907.
- (62) Szeto, C.-C.; Chan, R. W.-Y.; Lai, K.-B.; Szeto, C. Y.-K.; Chow, K.-M.; Li, P. K.-T.; Lai, F. M.-M. *Nephrol. Dial. Transplant.* **2005**, *20*, 105–113.
- (63) Reich, H. N.; Landolt-Marticorena, C.; Boutros, P. C.; John, R.; Wither, J.; Fortin, P. R.; Yang, S.; Scholey, J. W.; Herzenberg, A. M. *J. Mol. Diagn.* **2011**, *13*, 143–151.